IOP Publishing New J. Phys. 25 (2023) 093038 https://doi.org/10.1088/1367-2630/acf72c

New Journal of Physics
The open access journal at the forefront of physics

Deutsche Physikalische Gesellschaft DPG
IOP Institute of Physics

Published in partnership with: Deutsche Physikalische Gesellschaft and the Institute of Physics

OPEN ACCESS

RECEIVED
1 June 2023

REVISED
22 August 2023

ACCEPTED FOR PUBLICATION
6 September 2023

PUBLISHED
22 September 2023

PAPER

Optical deceleration of atomic hydrogen

S F Cooper*, C Rasor, R G Bullis, A D Brandt[1] and D C Yost

Colorado State University, 1875 Campus Delivery, Fort Collins, CO 80523, United States of America
[1] Present address: Time and Frequency Division, National Institute of Standards and Technology, 325 Broadway, Boulder, CO 80305, United States of America.
* Author to whom any correspondence should be addressed.

E-mail: samuel.cooper@rams.colostate.edu

Keywords: atomic beam, deceleration, atomic hydrogen, atomic physics, optical lattice

Supplementary material for this article is available online

Abstract

We demonstrate control over the motional degrees of freedom of a cryogenic hydrogen atomic beam using an accelerating optical lattice. For our method, we load metastable atoms from a cryogenic beam into a moving optical lattice, decelerate the lattice, and observe a commensurate deceleration of the atoms. For this demonstration, hydrogen atoms are decelerated by about 20 m s^{-1} in a 40 ns slowing cycle, with a peak acceleration of $\approx 4 \times 10^8$ m s^{-2}. Since the optical lattice is governed by standard optoelectronics, this technique represents a robust platform for the motional control of hydrogen.

1. Introduction

The study of hydrogen has played an important role in modern physics and was instrumental in the discovery of quantum mechanics, the Dirac equation, and quantum electrodynamics (QED) [1]. In addition to this illustrious history, hydrogen spectroscopy remains a dynamic field which helps to determine the Rydberg constant and proton charge radius [2], tests bound-state QED [3], and can search for Beyond Standard Model Physics [4–6]. Additionally, with recent demonstrations of anti-hydrogen trapping and spectroscopy, a new line of investigation is possible whereby hydrogen can be compared to its antimatter counterpart [7–14]. Spectroscopic measurements have reached a very high level of precision, for example, the 1S-2S transition has been measured with an impressive fractional uncertainty of only 4.2×10^{-15} [15]. However, most precision hydrogen spectroscopy is conducted with atomic beams with temperatures between 4.5 K and room temperature [15–20]—at least six orders of magnitude larger than what is routinely achieved in heavier atomic species through laser cooling [21]. This relatively high temperature often limits the measurement uncertainty, as in the 1S-2S measurement [15], which has motivated continued research into new methods to laser cool and decelerate hydrogen beams. The most conceptually simple method to laser cool hydrogen is through the 1S-2P cycling transition using Lyman-α radiation at 121.6 nm. However, Lyman-α radiation is very challenging to produce and manipulate [22–25]. Therefore, while laser cooling of hydrogen and antihydrogen has been demonstrated [22, 26], it is still far from routine. This has motivated other methods to achieve ultracold atomic hydrogen such as pulsed two-photon Doppler cooling [27], pulsed Sisyphus cooling [28], or photodissociation of trapped hydride molecules [29, 30]. In addition, there have been methods proposed [31, 32] and demonstrated [33] to decelerate supersonic hydrogen beams using pulsed magnetic fields.

An intriguing option for the deceleration of atomic or molecular beams is to use the optical dipole force [34–37]. However, to the best of our knowledge this has been experimentally unexplored with atomic hydrogen (although the pulsed Sisyphus method proposed in [28] does rely in part on the dipole force). This is likely because large dipole forces are typically only achievable with radiation which is nearly resonant to an electronic transition and, for ground-state hydrogen, these transitions are in the vacuum-ultraviolet spectral region, which would introduce challenges similar to those for laser cooling.

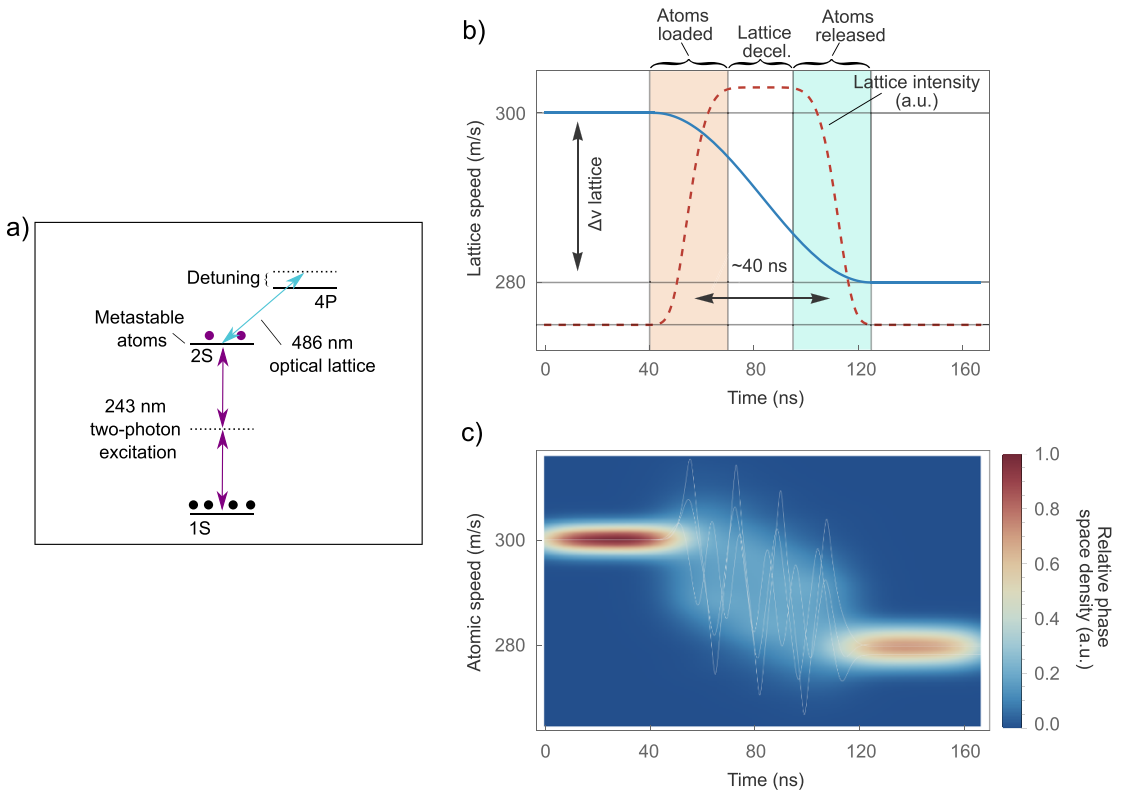

Figure 1. Method for the optical deceleration of atomic hydrogen. (a) Simplified energy level diagram showing relevant levels. After excitation to the 2S state using two photon excitation, an optical lattice is introduced using light nearly resonant with the 2S-4P transition. (b) Timing of our slowing method. The lattice intensity is shown in red, whereas the lattice velocity is shown in blue. The red shaded region shows the loading phase where atoms comoving with the lattice at 300 m s^{-1} are captured. The lattice is then decelerated to slow the trapped atoms before the lattice intensity is ramped down in the blue shaded region. (c) Density plot of Monte Carlo simulated trajectories over the course of a deceleration pulse for atoms with an initial velocity near 300 m s^{-1}. The colors represent the atomic densities in phase space. As the lattice decelerates from 300 m s^{-1} to 280 m s^{-1} the atoms oscillate within the wells of the optical lattice before their release. Three example atomic trajectories (white tracks) overlay the density plot.

Here, we circumvent these challenges by first exciting our atomic beam to the metastable 2S state (lifetime ∼122 ms). With that, there are several electronic transitions which can be accessed with visible lasers producing large optical forces. For the experiments described in this letter we use high-power (∼1 W) continuous-wave laser radiation at 486 nm which is nearly resonant with the 2S-4P transition. Our deceleration method uses a moving optical lattice in the path of our metastable hydrogen atomic beam. The slowing consists of three steps which are shown in figure 1. First, the lattice intensity is quickly turned on, trapping a fraction of the atoms. For this step, the speed of the lattice is set near the peak speed of the atomic beam, and the fraction of the velocity distribution trapped is determined by the depth of the lattice wells. The lattice is then decelerated, which produces a corresponding deceleration of the trapped atoms. Finally, the lattice is quickly turned off, leaving the atoms with a reduced speed. For our demonstration, atoms moving at speeds of roughly 300 m s^{-1} ± 15 m s^{-1} are trapped in the lattice wells and are then decelerated by about 20 m s^{-1} in a 40 ns slowing cycle. Atoms outside of this 30 m s^{-1} velocity range will typically travel between many lattice sites and are usually left with a slightly increased velocity following the slowing procedure.

2. Method

The design of our slowing process was determined using simple atomic physics arguments. For these estimates, we ignore fine and hyperfine structure and consider only the 2S and 4P levels. For an optical lattice which is far-detuned from the 2S-4P resonance, the maximum lattice potential due to the AC stark shift of the 2S level, which arises from the dipole interaction with the 4P state, is given by

$$U_{\max} = \hbar \frac{|\,\Omega_{\max}\,|^2}{4\delta}, \tag{1}$$

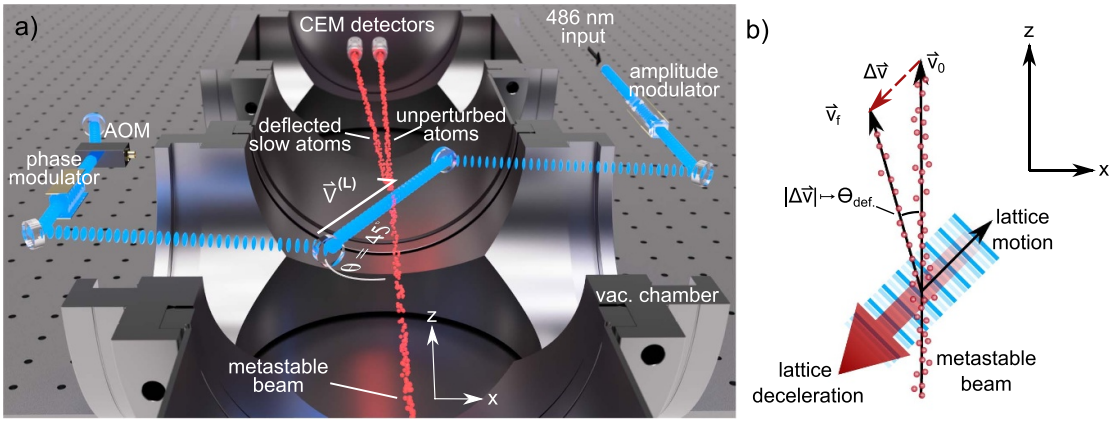

Figure 2. Experimental setup. (a) Balmer-β light (486 nm) first passes through an amplitude modulator which controls the lattice intensity. The light then passes through the interaction region before being retroreflected. The retroreflected beam is double-passed through an AOM to establish a central lattice velocity, and a phase modulator to provide the lattice acceleration. The lattice is placed at a 45° angle to the atomic beam so that the lattice simultaneously slows atoms along the beam axis (the z direction) and deflects them in the x direction. Two detectors count metastable atoms. One is placed on axis to provide normalization, and a second is placed at $\vec{x} = (2, 0, 27)$ cm after the deceleration region ($\theta_{\text{def.}} = 4.2°$). (b) To good approximation the optical lattice only exerts a force along its propagation direction. This means the 45° angle between the metastable beam and optical lattice the lattice will provide a velocity kick of equal magnitude to the x and z directions of the beam. Atoms with initial velocity of $\vec{v}_i = (0, 0, 300)$ m s^{-1} have a final velocity of $\vec{v}_f = (20, 0, 280)$ m s^{-1}, which is a change from $|\vec{v}_i| = 300$ m s^{-1} to $|\vec{v}_f| = 280.7$ m s^{-1} (approximately a deceleration of 20 m s^{-1}) that is visible to the off-axis detector.

where Ω_{max} is the maximum Rabi frequency, and δ is the detuning from the resonance in angular frequency units [38]. From this, it is clear that a larger well-depth can be obtained by increasing Ω_{max}, or decreasing δ. In general, it is desirable to maximize U_{max} to slow a larger fraction of the thermal atomic beam's velocity distribution. However, it is also important to consider quenching of the metastable 2S state via spontaneous emission. The dipole force originates from a small mixing of the 2S and 4P states, and the 4P state can decay to the ground 1S state. Once an atom is in the ground state, it ceases to be affected by the dipole forces from the optical lattice. Therefore, an optimized slowing process should be designed to minimize quenching of the 2S state while maximizing the optical lattice potential well depth. The maximum quench rate from off resonant excitation is given by

$$\Gamma_{\text{quench}} = \frac{|\,\Omega_{\text{max}}\,|^2}{4\delta^2}\gamma_{4P}, \tag{2}$$

where γ_{4P} is the decay rate from the 4P state. Since the quenching is suppressed by an additional factor of δ, it is possible to achieve the same lattice depth and a reduced quenching rate with more laser power and increased δ. In addition, it is advantageous to apply short deceleration pulses to limit quenching of the metastable atoms.

2.1. Experimental setup

Our hydrogen source is a cryogenic atomic beam (5 K), which has a peak velocity near 458 m s^{-1} [39]. The generation and characterization of our continuous effusive cryogenic beam of 2S hydrogen is described in previous works [20, 39–41]. Laser radiation at 243 nm crosses the atomic beam to excite the 1S-2S two-photon transition producing a metastable beam of 2S hydrogen [20, 39, 40]. The 2S hydrogen then travels for approximately 15 cm before arriving at the deceleration region. Here, the atomic beam crosses an optical lattice produced with ∼1 W of retroreflected, intensity-controlled, laser radiation at 486 nm. The slowing laser at 486 nm has not been previously described and begins with an extended cavity diode laser at 972 nm in the Littrow configuration. The output is amplified with a commercial tapered amplifier (DILAS), and frequency doubled to 486 nm using an AR coated lithium triborate (LBO) crystal in a resonant bowtie cavity. The 486 nm source produced ≈970 mW of CW power. After the optical losses from beam shaping and the Pockels cell, approximately 750−850 mW power was available for the decelerator. We measured 600 mW of backward going power due to losses in the double-pass acoustic-optic modulator (AOM) and electro-optic modulator (EOM). The radiation is focused to an 80 μm spot size at the atomic interaction region. As an aside, we previously demonstrated 4.2 W at 486 nm in [41]. As shown in figure 2, the optical lattice is oriented at a 45° angle with respect to the z-axis (i.e. the initial atomic beam propagation direction).

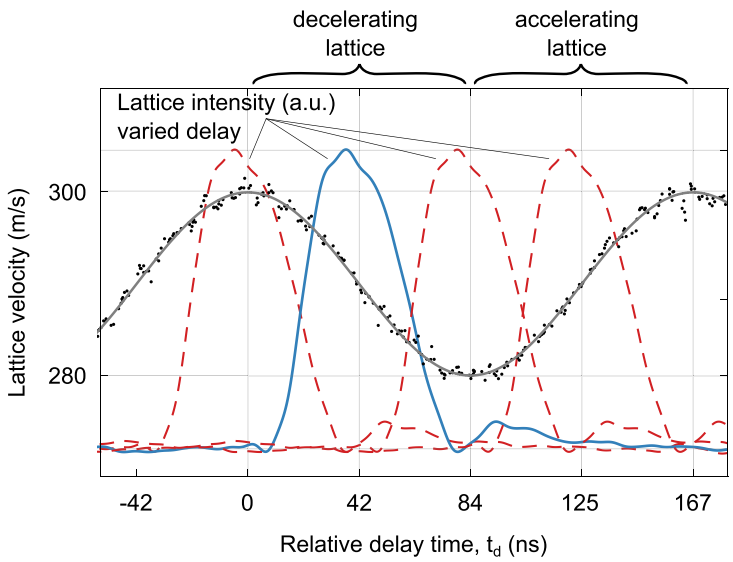

Figure 3. Experimental control of the optical lattice. The black data points show the measured sinusoidal modulation of the lattice velocity (black data points, grey fit) in the direction of the atomic beam. The time t_d is the relative delay between the peak of the lattice velocity and the lattice intensity, which can be varied using RF electronics. The solid blue trace corresponds to the normal operation of the decelerator where the lattice intensity is maximized as the lattice velocity is decreasing.

With this, the atoms receive a horizontal deflection in the x-direction as they are being slowed. This allows for a convenient method to detect the slowed fraction of the atomic beam with reduced background. Metastable hydrogen is readily detected with a simple channel electron multiplier (CEM) [20]. We use two such detectors—one in the direction of the initial atomic beam, and a second off-axis which is set to detect the slowed and deflected atoms. The on-axis CEM provides a normalization signal.

One of the attractive features of this slowing technique is that the lattice acceleration and intensity are precisely controlled with commercially available optoelectronic devices and RF electronics. To demonstrate and characterize the control of this technique we vary relative timing delay between the peak lattice intensity and the peak lattice velocity, t_d. With this, the lattice can be accelerating, decelerating, or held stationary during the pulse. The experimentally measured lattice intensity and lattice velocity are shown in figure 3 for several values of t_d. We then measured the number of counts on the off-axis atom detector while varying this delay, holding all other parameters constant. When the pulse has a delay of $t_d = 42$ ns the lattice is decelerating, which reproduces the desired operation of our deceleration scheme as depicted in figure 1.

An AOM and EOM in the retroreflected path allows for precise control of the velocity and acceleration of the optical lattice. In practice, the AOM sets a central lattice velocity and a sinusoidal phase modulation is applied to the EOM to produce the lattice acceleration. To apply the frequency chirp and accelerate the lattice, the beam is double passed through a 3 mm × 3 mm × 20 mm long y-cut phase modulation EOM made from magnesium doped lithium niobate with $r_{33} = 32$ pm V^{-1}. The EOM is operated as a phase modulator and is resonantly driven by a step-up transformer at 6 MHz. Figure 3 shows the measured lattice acceleration and variable timing of the lattice intensity pulse. Optimal selection of the decelerating region of the lattice speed is accomplished by aligning the peak of the lattice intensity with the decelerating portion of the phase modulation signal, as shown in figure 3.

Due to the double passed AOM and EO phase modulator, the retroreflected 486 nm radiation is shifted by a variable frequency, Δf, of between 815 MHz and 872 MHz. This produces a corresponding lattice well speed, given by $|\vec{v}^{(L)}| = \Delta f/2 \times 486$ nm, of between 212 m s^{-1} and 198 m s^{-1}. However, since the lattice is oriented at 45° with respect to the z-axis (the atomic beam direction), the lattice velocity with respect to that axis is more relevant. This is given by $v_z^{(L)} = \sqrt{2}\,|\vec{v}^{(L)}|$, which varies from 300 m s^{-1} to 280 m s^{-1}. Because the optical lattice may only exert a force along its propagation direction, the 45° angle between the metastable beam and optical lattice the lattice will provide a momentum kick of equal magnitude to the x and z directions of the beam. Atoms with initial velocity of $\vec{v}_i = (0, 0, 300)$ m s^{-1} obtain a final velocity $\vec{v}_f = (20, 0, 280)$ m s^{-1} after a trap-slow-release deceleration sequence is applied. This causes a change in speed from $|\vec{v}_i| = 300$ m s^{-1} to $|\vec{v}_f| = 280.7$ m s^{-1}, which is the only signal visible to the off-axis detector. Therefore detection of deflected atoms in the off-axis detector provides a clear demonstration of deceleration by ≈20 m s^{-1}.

The 486 nm radiation is focused to a spot size of 80 μm and is tuned to within about 1.2 GHz of the 2S-4P transition. With this lattice intensity and detuning, atoms which are traveling within ± 15 m s^{-1} of the initial lattice speed can be trapped within the lattice wells (roughly 13 mK lattice depth). As shown in figure 2, we can precisely control the depth of the optical lattice or turn it off completely using an electro-optic amplitude modulator on the 486 nm radiation before it reaches the slowing region. Our metastable beam is continuous and since it takes roughly 1 μs for the atomic beam to traverse the slowing region, the slowing procedure is repeated at a rate of 1 MHz. With this, a given decelerated atom is allowed to exit the interaction region before the next deceleration sequence is applied to a new set of atoms, generating a near-continuous slowed beam of metastable atoms.

3. Results and discussion

Figure 4 shows the slowed atom signal in the off-axis detector as a function of $t_{\rm d}$, where each data point corresponds to an integration time of 5 s. As expected, we observe a peak in the slowed-atom signal when the lattice is pulsed on as it is decelerating ($t_{\rm d} = 42$ ns). With this timing, the signal measured by the off-axis channeltron is regularly $\sim$100 counts per second which corresponds to roughly 5% of the slowable atoms (i.e. within 30 m s^{-1} near the central lattice velocity) in the measured velocity distribution [39]. This detected fraction coincides with the expected amount since our metastable atomic beam is roughly 350 μm in height whereas the optical lattice is only roughly 80 μm in height. The agreement between the simulated and experimental signal support that the atomic motion is dominated by the optical lattice. It is also useful to note that the neither the amplitude nor the alignment and phase of the lattice were stabilized as it is expected amplitude noise would only lead to small deviations in the trap depth and phase noise would be negligible compared to the significant lattice deceleration. When varying the pulse timing, we see a minimum in the slowed-atom signal when the lattice is pulsed on with no acceleration ($t_{\rm d} = 0$ and 84 ns). Interestingly, we also see a significant slowed-atom signal when lattice has a positive acceleration ($t_{\rm d} = 125$ ns) in the direction of the atomic beam velocity when it is pulsed on. While initially surprising, this behavior can be understood intuitively. For an atom to be localized at a single lattice site, an atom must be within 30 m s^{-1} of the initial lattice velocity. An atom which is slightly faster than this will travel between several lattice sites. However, if the lattice is accelerating in the same direction as the atomic velocity, then at some point in the interaction, the atom could be traveling with a peak speed only slightly faster than the lattice and will be reflected from the side of the nearest lattice well. This results in a negative impulse to the atom even when the lattice has a positive acceleration. This behavior is similar to the slowing observed when atoms are reflected from a moving surface [42].

To gain insight into this behavior, we performed a Monte Carlo (MC) simulation of the slowing process. The atomic motion in the presence of the time-dependent lattice potential, $U(\vec{r},t)$, was treated classically and the AC Stark shifts were calculated by diagonalizing the interaction Hamiltonian. Recoil due to spontaneous emission is not considered in this work since atoms which are excited to the 4P state are assumed to be lost. For these calculations, we include the 2S $F = 1$ levels and all fine and hyperfine levels in the 4P manifold. We include all fine structure splittings but ignore the 4P hyperfine splittings. The 2S $F = 0$ level is not considered in our analysis due to the selective two-photon excitation to the 2S $F = 1$ states. The resulting AC Stark shift of the 2S level is an analytic function of the laser intensity and detuning which we use to calculate a time and spatially varying potential. We use this potential to simulate classical atomic trajectories.

We model the lattice intensity as

$$I(\vec{r},t) = I_0(1+\eta^2+2\eta\cos(\Phi(z,t)))e^{-(r/w_0)^2}e^{-((t-t_{\rm d})/t_w)^6}, \tag{3}$$

where I_0 is the peak laser intensity, Φ is the axial phase of the standing wave interference pattern, w_0 is the Gaussian beam width and η^2 is the ratio of the backward to forward propagating laser power. In general, $\eta \neq 1$ because the double-passed AOM and EOM each have a non-negligible optical loss. Since the lattice is pulsed, we include a super-Gaussian temporal function centered at $t_{\rm d}$ and having a duration of t_w. The axial phase in equation (3) is given by

$$\Phi(z,t) = 2kz - \omega_\Delta t + \Phi_c \sin(2\pi f_c t), \tag{4}$$

where ω_Δ is the frequency difference produced by the AOM, and Φ_c and f_c are the respective modulation amplitude and frequency produced by the EOM. The position of the lattice intensity pulse with respect to the velocity modulation is controlled by the time delay, $t_{\rm d}$. The speed of the lattice is given by

$$v^{(\rm L)}(t) = v_{\rm l} + v_c \cos(2\pi f_c t), \tag{5}$$

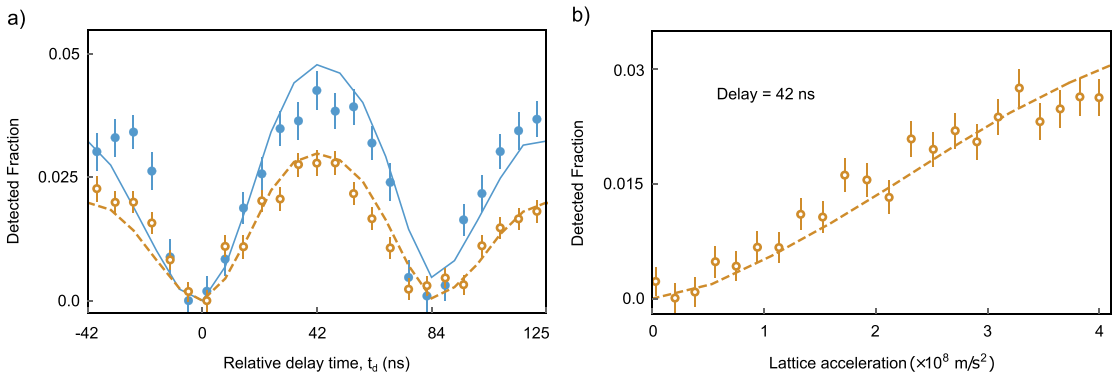

Figure 4. Observation of slowed-atom signal as function of lattice parameters. (a) Measured fraction of atomic beam deflected into the off-axis detector as a function of t_d. Blue solid points were taken at a detuning of $\delta = 2\pi \times 1.2 \times 10^9\,\mathrm{s}^{-1}$, a central lattice velocity of $v_z^{(L)} = 274\,\mathrm{m\,s}^{-1}$, and a peak lattice acceleration of $4 \times 10^8\ \mathrm{ms}^{-2}$. The solid blue line shows a simulation for the same experimental conditions. The yellow hollow data points were taken at a detuning of $\delta = 2\pi \times 1.5 \times 10^9\mathrm{s}^{-1}$, with a central lattice velocity $v_z^{(L)} = 307\,\mathrm{m\,s}^{-1}$, and a peak lattice acceleration of $4 \times 10^8\mathrm{m\,s}^{-2}$. The dashed yellow line shows a simulation for these same experimental conditions. (b) The off-axis signal as a function of the peak lattice acceleration. Data and simulation are for the same conditions as the yellow hollow points in (a). In both plots, the detected fraction is relative to the number of atoms within 30 m s^{-1} velocity near the central lattice velocity—i.e. the number of trappable atoms. This fraction was determined with the velocity distribution measured in [39]. Each data point is measured with 5 s of integration time and the error bars are calculated from the shot noise. All simulations use only experimental conditions (measured phase modulation to frequency chirp amplitude, metastable atomic beam size, AOM and EOM frequencies of ≈843 MHz, laser power and spot size of 800 mW and 80 μm respectively) with no free fit parameters.

where we have introduced the central lattice velocity $v_l = \omega_\Delta/(2k)$, and the amplitude of velocity modulation $v_c = \pi f_c \Phi_c/k$. The lattice acceleration is given by

$$a^{(L)}(t) = -a_0 \sin(2\pi f_c t), \tag{6}$$

where $a_0 = 2\pi f_c v_c$ is the acceleration amplitude. Experimentally, values for v_c, a_0 and v_l were measured *in situ* using a Michelson interferometer. We numerically integrated classical particle trajectories using these parameters for the optical lattice. To account for spontaneous emission loss to the ground state we also numerically integrated the steady-state optical Bloch equations for the population of $4P_{1/2}$ and $4P_{3/2}$ levels over the atomic trajectory through the optical lattice. Numerical simulations of millions of trajectories and survival probabilities are calculated over initial positions and velocities defined by our atomic beam [39]. We integrated our simulation over the initial atomic positions and velocities present in our hydrogen beam and the results of the simulation are shown in figure 4 overlapped with our experimental results. As can be seen in the figure, we achieve excellent agreement when our simulation is seeded with our experimental parameters.

To further explore the capabilities of this slowing technique, we performed simulations of a deceleration experiment which has 4.2 W of 486 nm laser power [41] focused to a 80 μm flat-top shaped intensity profile detuned by 8 GHz. We performed MC simulations for varied amounts of phase modulation (lattice velocity modulation) as shown in figure 5, allowing us to explore the relationship between the slowing cycle and the deceleration of hydrogen. A single stage of deceleration would be capable of bringing a group of atoms from the most probable velocity of 458 m s^{-1} to a stop. As shown by figure 5, although there is significant quenching of atoms that are not slowed, deceleration to a near standstill is possible without significant loss of 2S atoms through quenching. Atoms which are not trapped within the lattice are not slowed and experience larger average laser intensities, and thus more quenching, leading to a reduction in the final velocity distribution. However, because atoms that are loaded in the optical lattice sites spend much of their trajectory at the lowest intensities, the slowed portion of the distribution experiences minimal increase in quenching for increased deceleration as can be seen by minimal change in peak height of the slowed atoms in figure 5(c). It is interesting to note that atoms slower than the lattice initial velocity are heated by approximately the lattice depth over a range of velocities approximately equal to the deceleration amount, whereas atoms moving faster than the initial lattice velocity are mostly unaffected. We believe this is a direct result of the non-dissipative nature of our slowing since spontaneous emission does not play an active role in the slowing.

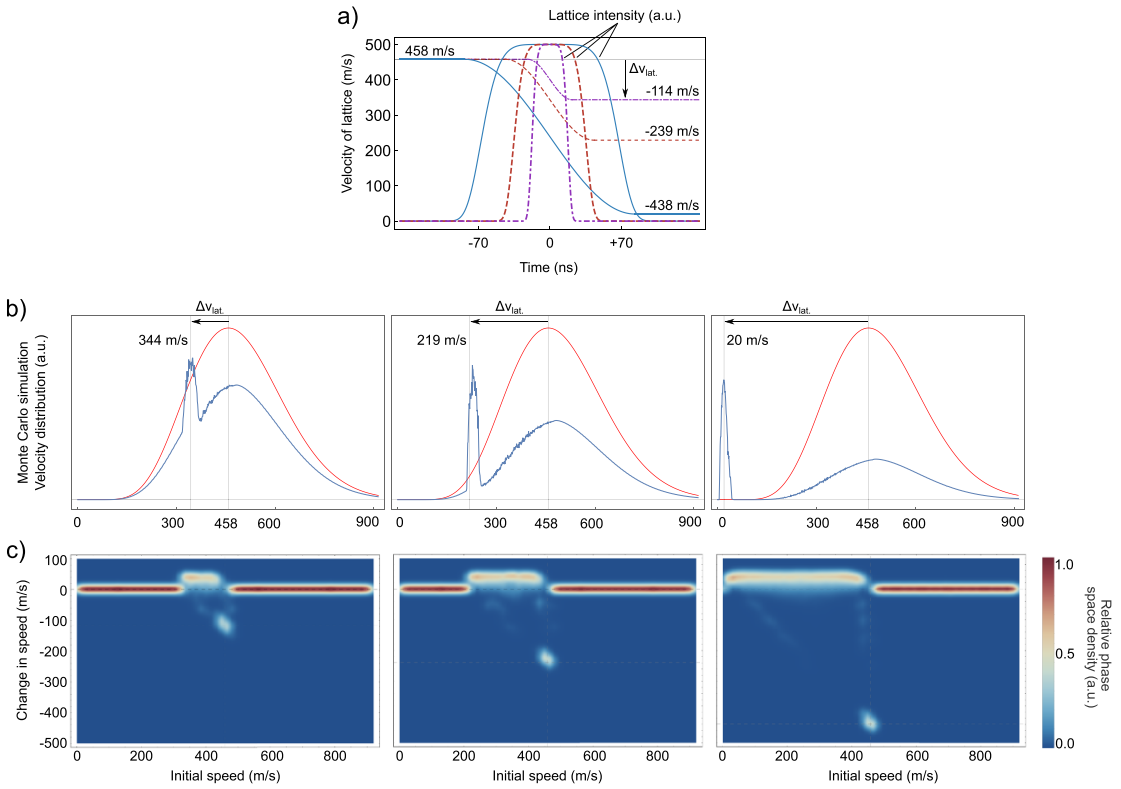

Figure 5. Simulation results using 4.2 W of 486 nm [41] detuned by 8 GHz and with a greater change in lattice velocity. With this, up to 438 $\mathrm{m\,s^{-1}}$ of slowing is obtained when using the same Monte Carlo (MC) simulation reproducing the experimental results in figure 4. (a) Slowing cycle for deceleration amounts of 114 $\mathrm{m\,s^{-1}}$ (purple dot-dashed pulse), 239 $\mathrm{m\,s^{-1}}$ (red dashed pulse), and 438 $\mathrm{m\,s^{-1}}$ (blue solid pulse), all starting at the most probable metastable velocity of 458 $\mathrm{m\,s^{-1}}$. (b) The initial velocity distributions shown in red were measured in [39]. The unslowed metastables distribution is reduced for increased deceleration because atoms which are not trapped within the lattice are not slowed, but are also quenched more due to a larger interaction time. The slowed portion of the beam spends more time at low intensity regions of the lattice and experiences a minimal increase in quenching for greater deceleration. (c) Effect on phase space for varied slowing amounts. The atoms residing in phase space near the initial lattice velocity are slowed by the deceleration of the lattice. Atoms faster than this are not perturbed, whereas atoms below the velocity of the lattice have a slightly increased speed.

4. Conclusion

The slowing method demonstrated in this letter is flexible and can be implemented to slow without deflection, or even placed at an angle to the vertical plane to deflect atoms into a fountain style trajectory to perform Ramsey spectroscopy [43]. Here we demonstrate a reduction in the kinetic energy of slowed atoms by roughly 12%. With additional lattice intensity it is clearly possible to reach a larger deceleration or the slowing of a larger portion of our velocity distribution without additional quenching given the simple atomic physics arguments above. Previously, we have demonstrated 4.2 W of optical power at 486 nm enabled with a Yb fiber amplifier [41], which could greatly improve performance and was used for the simulations shown in figure 5. In addition, it is notable that by using a CW laser along with an intensity modulator with a low duty cycle, 95% of the optical power is not used for slowing. Therefore, it is interesting to consider the use of a specially designed Q-switched laser to efficiently use the optical power available. However, the use of a CW laser as demonstrated here is more flexible since we have full control over the lattice intensity and pulse duration with relatively simple electronics.

Slow atomic samples of hydrogen could improve the precision of hydrogen spectroscopy, and in turn, yield increased sensitivity for tests of fundamental physics. Since the highest precision spectroscopy measurements of hydrogen have been performed with atomic beams with temperatures >4.5 K, this work could drastically improve the systematic uncertainties related to atomic velocity in these types of measurements. In addition, this slowing method could be used to load a magnetic atomic trap [33] or an optical dipole trap (see for example [44]). Finally, it is interesting to note that exotic atomic systems such as anti-hydrogen [12, 45], and muonium [46–49] have identical, or near-identical, energy level structure as

hydrogen. Therefore, the challenges in the optical manipulation of the motion of these atoms are similar to hydrogen.

Data availability statement

All data that support the findings of this study are included within the article (and any supplementary files).

Acknowledgments

The authors gratefully acknowledge funding of this project through NSF Grant #1654425. In addition, we would like to thank Jacob Roberts and Samuel Brewer for useful conversations, and Mingzhong Wu for the loan of RF test equipment.

ORCID iD

S F Cooper https://orcid.org/0000-0002-5173-1693

References

[1] Lamb W E and Retherford R C 1947 Fine structure of the hydrogen atom by a microwave method *Phys. Rev.* **72** 241–3
[2] Tiesinga E, Mohr P J, Newell D B and Taylor B N 2021 Codata recommended values of the fundamental physical constants: 2018 *Rev. Mod. Phys.* **93** 025010
[3] Karshenboim S G 2005 Precision physics of simple atoms: QED tests, nuclear structure and fundamental constants *Phys. Rep.* **422** 1–63
[4] Karshenboim S G 2010 Precision physics of simple atoms and constraints on a light boson with ultraweak coupling *Phys. Rev. Lett.* **104** 220406
[5] Yang Q and Dong S 2022 Probe dark matter axions using the hyperfine structure splitting of hydrogen atoms (arXiv:1912.11472)
[6] Jones M P A, Potvliege R M and Spannowsky M 2020 Probing new physics using Rydberg states of atomic hydrogen *Phys. Rev. Res.* **2** 013244
[7] Bluhm R, Kostelecký V A and Russell N 1999 *CPT* and Lorentz tests in hydrogen and antihydrogen *Phys. Rev. Lett.* **82** 2254–7
[8] Storry C H *et al* (ATRAP Collaboration) 2004 First laser-controlled antihydrogen production *Phys. Rev. Lett.* **93** 263401
[9] Andresen G B *et al* 2010 Trapped antihydrogen *Nature* **468** 673–6
[10] Gabrielse A *et al* (ATRAP Collaboration) 2012 Trapped antihydrogen in its ground state *Phys. Rev. Lett.* **108** 113002
[11] Kostelecký V A and Vargas A J 2015 Lorentz and *CPT* tests with hydrogen, antihydrogen and related systems *Phys. Rev.* D **92** 056002
[12] Malbrunot C *et al* 2018 The ASACUSA antihydrogen and hydrogen program: results and prospects *Phil. Trans. R. Soc.* A **376** 20170273
[13] Ahmadi M *et al* 2018 Characterization of the 1S-2S transition in antihydrogen *Nature* **557** 71–75
[14] The ALPHA Collaboration 2020 Investigation of the fine structure of antihydrogen *Nature* **578** 375–80
[15] Parthey C G *et al* 2011 Improved measurement of the hydrogen $1S-2S$ transition frequency *Phys. Rev. Lett.* **107** 203001
[16] Beyer A *et al* 2017 The Rydberg constant and proton size from atomic hydrogen *Science* **358** 79–85
[17] Fleurbaey H, Galtier S, Thomas S, Bonnaud M, Julien L, Biraben F, Nez F, Abgrall M and Guéna J 2018 New measurement of the $1S-3S$ transition frequency of hydrogen: contribution to the proton charge radius puzzle *Phys. Rev. Lett.* **120** 183001
[18] Bezginov N, Valdez T, Horbatsch M, Marsman A, Vutha A C and Hessels E A A 2019 Measurement of the atomic hydrogen lamb shift and the proton charge radius *Science* **365** 1007–12
[19] Grinin A, Matveev A, Yost D C, Maisenbacher L, Wirthl V, Pohl R, Hänsch T W and Udem T 2020 Two-photon frequency comb spectroscopy of atomic hydrogen *Science* **370** 1061–6
[20] Brandt A D, Cooper S F, Rasor C, Burkley Z, Matveev A and Yost D C 2022 Measurement of the $2S_{1/2}-8D_{5/2}$ transition in hydrogen *Phys. Rev. Lett.* **128** 023001
[21] Letokhov V S, Ol'shanii M A and Ovchinnikov Y B 1995 Laser cooling of atoms: a review *Quantum Semiclass. Opt.* **7** 5–40
[22] Hijmans T W, Luiten O J, Setija I D and Walraven J T M 1989 Optical cooling of atomic hydrogen in a magnetic trap *J. Opt. Soc. Am.* B **6** 2235–43
[23] Eikema K S E, Walz J and Hänsch T W 2001 Continuous coherent Lyman-α excitation of atomic hydrogen *Phys. Rev. Lett.* **86** 5679–82
[24] Michan J M, Fujiwara M C and Momose T 2014 Development of a Lyman-α laser system for spectroscopy and laser cooling of antihydrogen *Hyperfine Interact.* **228** 77–80
[25] Gabrielse G *et al* 2018 Lyman-α source for laser cooling antihydrogen *Opt. Lett.* **43** 2905
[26] Baker C J *et al* 2021 Laser cooling of antihydrogen atoms *Nature* **592** 35–42
[27] Kielpinski D 2006 Laser cooling of atoms and molecules with ultrafast pulses *Phys. Rev.* A **73** 063407
[28] Wu S, Brown R C, Phillips W D and Porto J V 2011 Pulsed sisyphus scheme for laser cooling of atomic (anti)hydrogen *Phys. Rev. Lett.* **106** 213001
[29] McNally R L, Kozyryev I, Vazquez-Carson S, Wenz K, Wang T and Zelevinsky T 2020 Optical cycling, radiative deflection and laser cooling of barium monohydride (^{138}Ba^{1}H) *New J. Phys.* **22** 083047
[30] Vázquez-Carson S F, Sun Q, Dai J, Mitra D and Zelevinsky T 2022 Direct laser cooling of calcium monohydride molecules *New J. Phys.* **24** 083006
[31] Raizen M G 2009 Comprehensive control of atomic motion *Science* **324** 1403–6
[32] Narevicius E, Libson A, Parthey C G, Chavez I, Narevicius J, Even U and Raizen M G 2008 Stopping supersonic beams with a series of pulsed electromagnetic coils: an atomic coilgun *Phys. Rev. Lett.* **100** 093003
[33] Hogan S D, Wiederkehr A W, Schmutz H and Merkt F 2008 Magnetic trapping of hydrogen after multistage Zeeman deceleration *Phys. Rev. Lett.* **101** 143001

[34] Dahan M B, Peik E, Reichel J, Castin Y and Salomon C 1996 Bloch oscillations of atoms in an optical potential *Phys. Rev. Lett.* **76** 4
[35] Fulton R, Bishop A I and Barker P F 2004 Optical stark decelerator for molecules *Phys. Rev. Lett.* **93** 243004
[36] Ramirez-Serrano J, Strecker K E and Chandler D W 2006 Modification of the velocity distribution of H_2 molecules in a supersonic beam by intense pulsed optical gradients *Phys. Chem. Chem. Phys.* **8** 2985–9
[37] Fulton R, Bishop A I, Shneider M N and Barker P F 2006 Controlling the motion of cold molecules with deep periodic optical potentials *Nat. Phys.* **2** 465–8
[38] Metcalf H J and van der Straten P 1999 *Laser Cooling and Trapping* (Springer)
[39] Cooper S F, Brandt A D, Rasor C, Burkley Z and Yost D C 2020 Cryogenic atomic hydrogen beam apparatus with velocity characterization *Rev. Sci. Instrum.* **91** 013201
[40] Cooper S F, Burkley Z, Brandt A D, Rasor C and Yost D C 2018 Cavity-enhanced deep ultraviolet laser for two-photon cooling of atomic hydrogen *Opt. Lett.* **43** 1375–8
[41] Burkley Z, Brandt A D, Rasor C, Cooper S F and Yost D C 2019 Highly coherent, Watt-level deep-UV radiation via a frequency-quadrupled Yb-fiber laser system *Appl. Opt.* **58** 1657–61
[42] Narevicius E, Libson A, Riedel M F, Parthey C G, Chavez I, Even U and Raizen M G 2007 Coherent slowing of a supersonic beam with an atomic paddle *Phys. Rev. Lett.* **98** 103201
[43] Huber A, Gross B, Weitz M and Hänsch T W 1998 Two-photon optical Ramsey spectroscopy of the $1S-2S$ transition in atomic hydrogen *Phys. Rev.* A **58** 2631–4
[44] Adhikari C M, Canales J C, Arthanayaka T P W and Jentschura U D 2022 Magic wavelengths for $1S$–nS and $2S$–nS transitions in hydrogen like systems *Atoms* **10** 1
[45] Malbrunot C *et al* 2019 Hydrogen beam to characterize the ASACUSA antihydrogen hyperfine spectrometer *Nucl. Instrum. Methods Phys. Res.* A **935** 110–20
[46] Janka G *et al* 2020 Intense beam of metastable muonium *Eur. Phys. J.* C **80** 804
[47] Crivelli P 2018 The Mu-MASS (muonium laser spectroscopy) experiment *Hyperfine Interact.* **239** 49
[48] Ohayon B *et al* 2022 Precision measurement of the lamb shift in muonium *Phys. Rev. Lett.* **128** 011802
[49] Delaunay C, Ohayon B and Soreq Y 2021 Towards an independent determination of muon $g-2$ from muonium spectroscopy *Phys. Rev. Lett.* **127** 251801